



# Weldability of aluminium-copper in explosive welding

G. H. S. F. L. Carvalho<sup>1</sup> · I. Galvão<sup>1,2</sup> · R. Mendes<sup>3</sup> · R. M. Leal<sup>1,4</sup> · A. Loureiro<sup>1</sup>

Received: 7 November 2018 / Accepted: 1 May 2019 / Published online: 12 May 2019  
© Springer-Verlag London Ltd., part of Springer Nature 2019

## Abstract

A large number of aluminium-copper explosive welds were produced under different welding conditions to perform a broad analysis of the weldability of this combination. The influence of the explosive mixture and the relative positioning of the plates on the welding results were analysed. When the aluminium alloy is positioned as the flyer plate, continuous interfacial melting occurred under the low values of energy lost by the collision, and collision point velocity. This proved that the weldability of the aluminium-copper combination is higher when the copper is positioned as the flyer. A mismatch between the experimental results and the existing theories that define the requirements for achieving consistent welds was noticed. Especially for welds produced using the aluminium alloy as the flyer, the experiments proved to be more restrictive than the theories. These theories, despite being widely applied in dissimilar welding literature, present several limitations concerning aluminium-copper welding. New approaches considering the formation of intermetallic phases at the interface, the properties of both welded metals, and/or the difference in their properties should be developed.

**Keywords** Explosive welding · Aluminium · Copper · Intermetallic phases · Solid-state welding · Kinetic energy

## 1 Introduction

Explosive welding (EXW) is a solid-state welding technology presenting a high potential for joining materials with very different physical properties and/or alloys that form intermetallic phases easily. As it is a very short cycle process, the interaction of the metals under high temperature and strain is reduced, preventing an extensive formation of intermetallic phases [1]. In addition, the region under the influence of the welding process is confined to a very narrow layer near the weld interface, promoting the formation of a very small heat-affected zone [2]. As shown in Table 1, intense research has been recently conducted in dissimilar EXW of aluminium alloys (Al) to other materials, such as carbon (CS) and stainless

steels (SS) and copper (Cu), magnesium (Mg), titanium (Ti), and nickel (Ni) alloys. In fact, the most recent design criteria are focused on multi-material components, which combine the specific properties of two or more materials.

Among the different dissimilar welding combinations, the Al-Cu is one of those with the highest interest to many industries. The production of components combining the low density and cost of Al with the excellent thermal and electric conductivities of Cu enables the development of new concepts and solutions. The most recent studies conducted in this area (Table 1) are essentially focused on understanding the interfacial phenomena occurring during welding and their influence on the final weld structure.

Paul et al. [7] conducted an investigation on the phase composition of Al-Cu joints. The authors reported the formation of three equilibrium intermetallic phases inside the solidified regions, i.e.  $\text{CuAl}_2$ ,  $\text{CuAl}$ , and  $\text{Cu}_9\text{Al}_4$ . These phases were found to be surrounded by dendrites of metastable phases. The distribution of the phases formed did not present a significant regularity inside the solidified regions. In turn, Athar and Tolaminejad [6] studied the influence of the explosive ratio (R), which is the ratio between the explosive and the flyer masses, on the interface properties of the welds. The wave amplitude and the amount of intermetallic phases were found to increase with increments in the explosive ratio. Regarding the mechanical behaviour of the welds, a higher

✉ R. Mendes  
ricardo.mendes@dem.uc.pt

<sup>1</sup> CEMMPRE, Department of Mechanical Engineering, University of Coimbra, Coimbra, Portugal

<sup>2</sup> ISEL, Department of Mechanical Engineering, Polytechnic Institute of Lisbon, Lisbon, Portugal

<sup>3</sup> ADAI, LEDAP, Department of Mechanical Engineering, University of Coimbra, Coimbra, Portugal

<sup>4</sup> ESAD.CR, Polytechnic Institute of Leiria, Leiria, Portugal

**Table 1** Recent research on dissimilar EXW of Al to other materials

Materials	Recent works
Al-Cu	Carvalho et al. [3], Carvalho et al. [4], Loureiro et al. [5], Athar and Tolaminejad [6], Paul et al. [7]
Al-Mg	Zhang et al. [8], Fronczek et al. [9], Arisova et al. [10], Zhang et al. [11]
Al-Ni	Guo et al. [12], Bataev et al. [13]
Al-Ti	Chulist et al. [14], Fan et al. [15], Bazarnik et al. [16], Fronczek et al. [17], Lazurenko et al. [18]
Al-CS	Carvalho et al. [19], Guo et al. [20], Aizawa et al. [21], Li et al. [22]
Al-SS	Carvalho et al. [23], Shiran et al. [24], Guo et al. [25], Xunzhong et al. [26]

shear strength was achieved for wavy interfaces without extensive formation of intermetallic regions. One year later, the influence of the explosive mixture on the quality of the welding results was addressed by Loureiro et al. [5]. These authors reported that the explosive sensitiser presents a strong influence on several aspects of the weld structure, such as the surface appearance and the morphology and the phase composition of the interface.

The morphology of the dissimilar interface was studied more profoundly by Carvalho et al. [4]. These authors concluded that the interface morphology is governed by the difference in the physical properties of the welded plates. According to them, when a much denser flyer with a much higher melting temperature than the baseplate is used, the formation of interfacial waves usually does not occur. More recently, Carvalho et al. [3] studied the influence of the flyer and baseplate properties on the welding results. The interaction of the materials was found to be completely different depending on how they are positioned in the joint (as flyer or as baseplate). These authors also reported that the formation of a continuous intermetallic layer along the weld interface promotes after-impact failure.

Although some works have already been conducted in Al-Cu joining by EXW, no broad weldability analyses exist in the literature, especially addressing the suitability of the tools and equations currently used to predict the welding results. Most of the existing research addresses a small number of welding conditions, which does not make it possible to reach global and generalizable conclusions on the weldability of this combination. So, the aim of this research, which combines an experimental and a theoretical approach, is to conduct a broad analysis of the weldability of the Al-Cu combination by EXW. A large number of welds were produced under different welding conditions. The influence of the explosive mixture and the relative positioning of the plates on Al-Cu welding results were studied.

## 2 Experimental procedure

Aluminium-copper welds were produced by EXW. The welded materials are presented in Table 2. As shown in the

table, plates with different thicknesses and two distinct Al alloys were welded.

The welds were produced in a parallel arrangement, with two joint designs: fully and partially overlapping. Some welds were produced with the Cu as the flyer plate and the Al alloy as the baseplate, while other welds were produced with the reverse positioning. The nomenclature used to label the welds indicates the flyer and the baseplates and their respective thickness. So, 1Cu/3Al identifies welds produced using a 1-mm-thick flyer plate of Cu and a 3-mm-thick baseplate of Al. Each weld is also characterised by a last digit which identifies the welding parameters used to produce it (e.g. 1Cu/3Al-1 and 1Cu/3Al-2).

The welding parameters concerning all the welds are displayed in Table 3. As shown in the table, a large range of parameters were tested to perform a broad analysis of the weldability of this combination of alloys. Different explosive ratios and stand-off distances (STD) were tested. An ammonium nitrate-based emulsion explosive (EE) and ANFO, which have significant different detonation velocities ( $V_d$ ), were used as the bases of the explosive mixtures. Some of the mixtures tested were sensitised with expanded polystyrene spheres (EPS) and others with hollow glass microspheres (HGMS) in order to obtain different explosive ratios and detonation velocities [27]. Other additives like aluminium powder could also be mixed with EE to change the detonation parameters [28].

The detonation velocity of the explosive mixtures was measured following the procedure reported in Mendes et al. [29]. As the welds were produced in parallel arrangement, the collision point velocity ( $V_c$ ) presents the same value as the detonation velocity. The impact velocity ( $V_p$ ) and the collision angle ( $\beta$ ) were calculated using the Gurney equation for a one-dimensional problem in parallel arrangement (Eq. 1) [1, 30] and with a relation between both

**Table 2** Welded materials

Welded materials	
Alloy	Thickness (mm)
AA5083	30
AA6082	3
Copper-DHP	1
	3

**Table 3** Welding parameters

Welds	Flyer (alloy, thicken.)	Baseplate (alloy, thicken.)	Explosive mixt.	STD	R
3Cu/30Al-1	Cu-DHP, 3 mm	AA5083, 30 mm	ANFO	3.7 mm	0.6
3Cu/30Al-2			ANFO	3.7 mm	0.9
1Cu/30Al-1	Cu-DHP, 1 mm	AA5083, 30 mm	ANFO+EE	1.4 mm	1.4
1Cu/30Al-2			ANFO	1.4 mm	1.8
1Cu/30Al-3			ANFO+EE	1.4 mm	2.3
1Cu/30Al-4			ANFO	1.4 mm	2.6
1Cu/3Al-1	Cu-DHP, 1 mm	AA6082, 3 mm	EE + EPS	1.4 mm	3.0
1Cu/3Al-2			EE + EPS	1.4 mm	4.3
1Cu/3Al-3			EE + HGMS	1.4 mm	1.7
1Cu/3Al-4			EE + HGMS	1.4 mm	2.1
3Al/3Cu-1	AA6082, 3 mm	Cu-DHP, 3 mm	ANFO	3.6 mm	2.0
3Al/3Cu-2			EE + EPS	4.0 mm	2.7
3Al/3Cu-3			EE + HGMS	3.6 mm	1.0
3Al/3Cu-4			EE + HGMS	3.6 mm	1.4
3Al/3Cu-5			EE + HGMS	4.0 mm	2.4
3Al/3Cu-6			EE + HGMS	1.4 mm	2.4
3Al/3Cu-7			EE + HGMS	4.0 mm	1.4
5Al/3Cu-1	AA6082, 5 mm	Cu-DHP, 3 mm	ANFO	6.2 mm	1.2

velocities and the impact angle (Eq. 2) [1]. The values measured for the detonation velocity and the values calculated for the impact velocity and impact angle are displayed in Table 4. The table also indicates the final welding result for each joint, labelling them as either failed or consistent. The failed welds were all the welds for which the plates were found to separate after the impact.

$$V_p = (2E)^{\frac{1}{2}} \left( \frac{3R^2}{R^2 + 5R + 4} \right)^{\frac{1}{2}} \tag{1}$$

$$\beta = 2 \arcsin \left( \frac{V_p}{2V_d} \right) \tag{2}$$

$(2E)^{\frac{1}{2}}$  is the Gurney characteristic velocity of each explosive ( $\text{m}\cdot\text{s}^{-1}$ ). An empirical correlation obtained by Cooper [31] for ideal explosives, i.e.  $(2E)^{\frac{1}{2}} = \frac{V_d}{2.97}$ , was used to estimate this parameter.

After welding, the welds were sectioned, and samples were removed longitudinally to the welding direction and prepared according to ASTM E3-11. The morphological characterisation of the welds was performed by optical microscopy, using an optical microscope, Leica DM4000M LED. The microstructural analysis was conducted by SEM, using a field emission scanning electron microscope, Zeiss Merlin VP Compact. This microscope was equipped with EDS, which was used to analyse the chemical composition of the welds.

### 3 Results and discussion

#### 3.1 Welding results

A graphical approach to the welding results is illustrated in Fig. 1. According to the positioning of the plates in the joint,

**Table 4** Values of collision point velocity, impact velocity, and impact angle

Welds	$V_d$ ( $\text{m}\cdot\text{s}^{-1}$ )	$V_p$ ( $\text{m}\cdot\text{s}^{-1}$ )	$\beta$ ( $^\circ$ )	Welding result
3Cu/30Al-1	1647	210	7.3	Consistent
3Cu/30Al-2	2072	350	9.7	Consistent
1Cu/30Al-1	1712	384	12.9	Consistent
1Cu/30Al-2	1855	481	14.9	Consistent
1Cu/30Al-3	2013	586	16.7	Consistent
1Cu/30Al-4	2149	673	18.0	Consistent
1Cu/3Al-1	2121	704	19.1	Consistent
1Cu/3Al-2	2271	859	21.8	Consistent
1Cu/3Al-3	3275	817	14.3	Consistent
1Cu/3Al-4	3430	974	16.3	Consistent
3Al/3Cu-1	2077	577	16.0	Consistent
3Al/3Cu-2	2987	947	18.2	Failed
3Al/3Cu-3	3256	596	10.5	Failed
3Al/3Cu-4	3256	726	12.8	Failed
3Al/3Cu-5	3477	1037	17.2	Failed
3Al/3Cu-6	3589	1072	17.2	Failed
3Al/3Cu-7	3665	823	12.9	Failed
5Al/3Cu-1	2077	435	12.0	Consistent

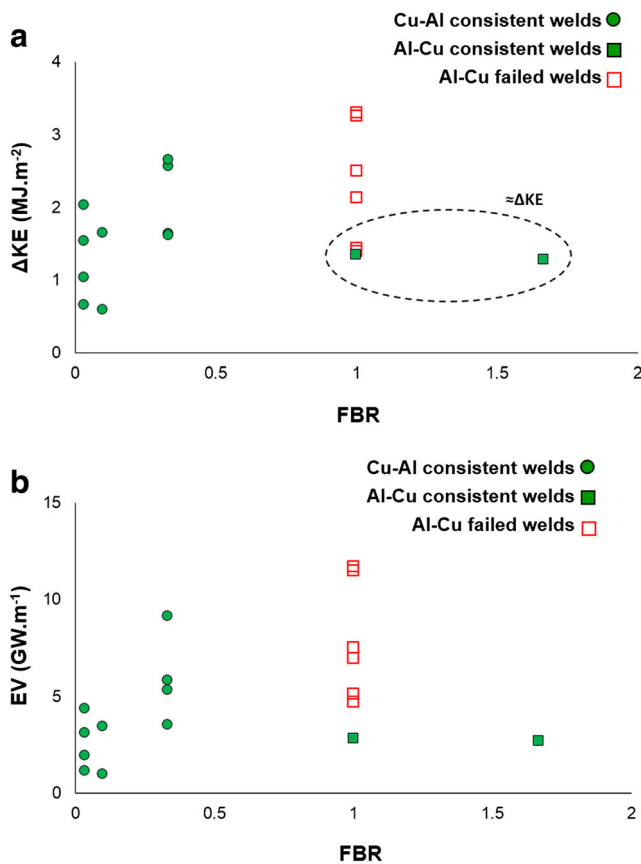


**Fig. 1** Graphical approach to the welding results. **a**  $\Delta KE$  vs FBR. **b** EV vs FBR

the welds are represented by circles (Cu/Al) or squares (Al/Cu). The green and red circles/squares correspond to consistent and failed welds, respectively. Figure 1 shows the kinetic energy lost in the collision ( $\Delta KE$ ) plotted according to the flyer to baseplate thickness ratio (FBR) for each weld. The  $\Delta KE$  has been used by several authors to assess the thermomechanical conditions experienced at the weld interface [32, 33]. This parameter was computed according to Eq. 3.

$$\Delta KE [J \cdot m^{-2}] = \frac{1}{2} m_{\text{flyer}} \cdot V_p^2 \quad (3)$$

$m_{\text{flyer}}$  is the mass per unit area ( $\text{kg} \cdot \text{m}^{-2}$ ) of the flyer plate;  $V_p$  is the impact velocity ( $\text{m} \cdot \text{s}^{-1}$ ).

The figure shows that all the Cu/Al welds presented consistent joining. On the other hand, consistent joining was not achieved in most of the welds produced with the reverse positioning of the plates. No consistent Al/Cu welds were achieved for  $\Delta KE$  values higher than  $1.5 \text{ M J} \cdot \text{m}^{-2}$ . In good agreement with Carvalho et al. [3], these results indicate that the relative positioning of the plates influences the weldability of the combination. However, different welding results were obtained for Al/Cu welds produced with similar  $\Delta KE$  values (indicated within the dashed ellipse in Fig. 1a). So, this parameter by itself

does not permit a full assessment of the thermomechanical conditions experienced at the dissimilar interface.

As reported by Carvalho et al. [19], the  $\Delta KE$  should be analysed together with the collision point velocity. High values of the  $\Delta KE$  and the collision point velocity favour interfacial melting, which in excess leads to after-impact failure [1]. So, the coupled effect of these two parameters on the interfacial conditions can be realised by calculating the EV parameter (Eq. 4), which corresponds to their product.

$$EV [W \cdot m^{-1}] = \Delta KE \cdot V_c = \frac{1}{2} m_{\text{flyer}} \cdot V_p^2 \cdot V_c \quad (4)$$

$m_{\text{flyer}}$  is the mass per unit area ( $\text{kg} \cdot \text{m}^{-2}$ ) of the flyer plate;  $V_p$  is the impact velocity ( $\text{m} \cdot \text{s}^{-1}$ );  $V_c$  is the collision point velocity ( $\text{m} \cdot \text{s}^{-1}$ ).

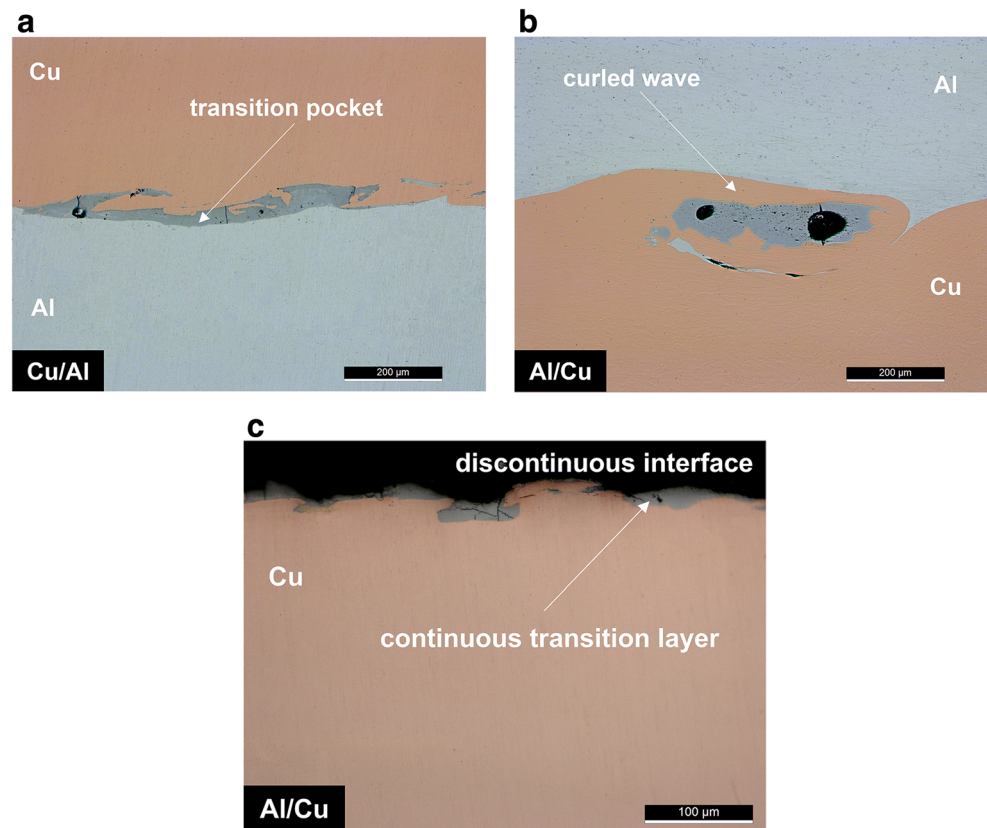
Figure 1 b shows the EV parameter plotted according to the FBR for each weld. As shown in the figure, this parameter allowed a better grouping of the failed welds than the  $\Delta KE$ , evidencing the very strong influence of the collision point velocity on the welding results. The failed welds present two characteristics: (i) the flyer plate was the Al alloy; (ii) the EV value was greater than  $4.5 \text{ GW} \cdot \text{m}^{-1}$ . These results make it possible to infer that two factors may contribute to reducing the weldability of the welded combination: the use of the Al alloy as the flyer plate and the use of a high EV value (high  $V_c$  and high  $\Delta KE$ ).

### 3.2 Weld interface morphology and structure

The morphology of the weld interfaces is displayed in Fig. 2. Three optical micrographs are presented in this figure, which concern a Cu/Al weld (Fig. 2a), a consistent Al/Cu weld (Fig. 2b), and a failed Al/Cu weld (Fig. 2c). As shown in Fig. 2 a, effective bonding was achieved at the interface of the Cu/Al welds, which presented a flat morphology. Localised transition pockets were formed along the interface of these welds. In turn, as illustrated in Fig. 2 b, the consistent Al/Cu welds presented the formation of interfacial curled waves, in which localised transition regions were observed. However, the morphology of most of the Al/Cu welds, which presented after-impact failure, is shown in Fig. 2 c. A continuous transition layer was always formed at the interface of the failed welds (both on the flyer plate and the baseplate after separation). The morphological characteristics of the different welds are in good agreement with the results from Carvalho et al. [3, 4].

SEM micrographs and EDS elemental maps of the transition regions of the Cu/Al and the consistent Al/Cu welds are illustrated in Fig. 3. From Fig. 3 a and b, it can be observed that the transition material displays a different morphology from the welded metals. Figure 3 c and d show that this material presents a mixed chemical composition, being composed of both Al and Cu. This chemical composition suggests the formation of new phases at the weld interface.

**Fig. 2** Optical micrographs of the weld interface. **a** Cu/Al weld. **b** Consistent Al/Cu weld. **c** Failed Al/Cu weld



Microstructural details of the weld interface are illustrated in Fig. 4. As shown in Fig. 4 a and b, solidified structures are present in the transition regions of the Cu/Al welds. Dendrites with different shapes, dispersed over a darker matrix, are observed in these zones. Table 5 presents the chemical distribution of aluminium and copper, showing that the composition of the dendrites (zone 1 in Fig. 4a and zone 4 in Fig. 4b) matches the chemical composition of the phase  $\text{CuAl}_2$  [34, 35]. Regarding the darker matrix, its chemical composition (zone 2 in Fig. 4a and zones 5 and 6 in Fig. 4b) does not match the composition of any equilibrium intermetallic phase, suggesting a mixture of Al and  $\text{CuAl}_2$  [34]. Moreover, an intermetallic phase nucleating from the Cu layer is also observed in Fig. 4a (zone 3). The Cu-rich composition of this phase (Table 5) matches the chemical composition of the  $\text{Cu}_9\text{Al}_4$  phase [34, 35]. Regarding the Al/Cu weld, the chemical analysis also suggests that the  $\text{CuAl}_2$  dendrites (zone 7 in Fig. 4c) are dispersed over an Al +  $\text{CuAl}_2$  matrix (zone 8 in Fig. 4c). Although a good match in chemical composition was obtained in some zones, it should be stressed that the main focus of this analysis is to show the formation of intermetallic phases at the weld interface rather than to accurately identify the specific phases, which is not possible by EDS.

These results make it possible to infer that intermetallic phases were formed at the interface of all welds. However, it was observed that no effective bonding can be achieved when

a continuous intermetallic layer forms at the weld interface. According to Carvalho et al. [3, 19], this layer results from excessive interfacial melting. As all the failed Al/Cu welds displayed a continuous interfacial layer, it can be concluded that these welds failed due to excessive melting. It should be stressed that, although some Al/Cu welds were produced with a lower EV than some Cu/Al welds, melting throughout the interface was only registered in Al/Cu welds (Fig. 1b).

### 3.3 Analysis of the welding conditions

To better understand the results, Al/Cu and Cu/Al welding configurations were analysed based on the concept of the weldability window. This tool is a graphical approach to the welding requirements to achieve consistent welds, which relates the collision point velocity to the collision angle [36]. It is composed of four limits. The left limit (*Cowan's limit*) defines the conditions required to achieve a wavy interface, and is calculated according to Eq. 5 [37]. The right limit (*Walsh's limit*) establishes the conditions required for the formation of an interfacial jet. It was plotted by assuming the maximum collision point velocity as the bulk sound speed in the material [38]. The lower limit (*Deribas and Zakharenko's limit*), which was calculated according to Eq. 6 [39], defines the minimum energy conditions to promote interfacial bonding. The upper limit (*Wittman's limit*) establishes the maximum energy

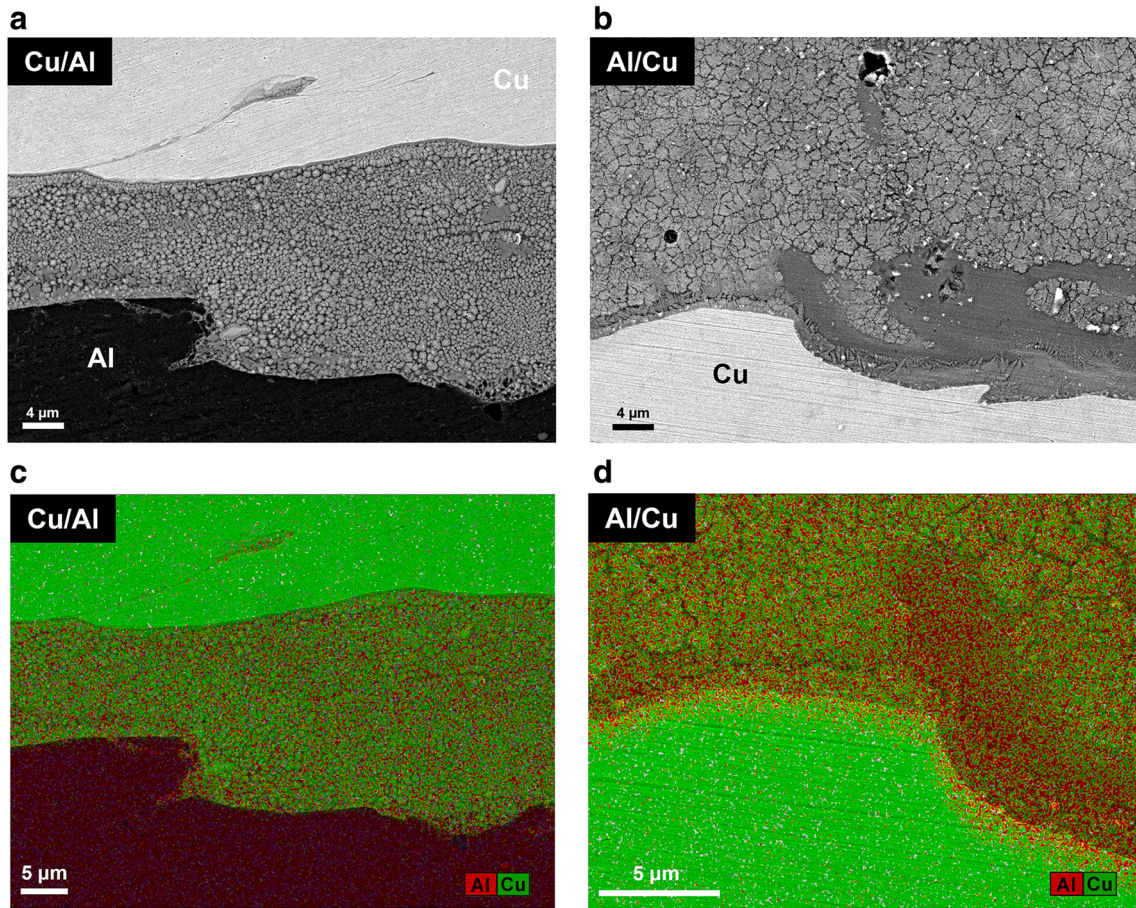


Fig. 3 SEM micrographs (top) and EDS elemental maps (bottom) of the weld interface. a, c Cu/Al weld. b, d Consistent Al/Cu weld

conditions to avoid excessive interfacial melting, and is calculated using Eq. 7 [40].

$$R_T = \frac{(\rho_{\text{flyer}} + \rho_{\text{base}}) V_c^2}{2(H_{\text{flyer}} + H_{\text{base}})} \quad (5)$$

$R_T$  is the Reynolds number,  $\rho_{\text{flyer}}$  and  $H_{\text{flyer}}$  are the density ( $\text{kg}\cdot\text{m}^{-3}$ ) and the hardness (Pa) of the flyer plate,  $\rho_{\text{base}}$  and  $H_{\text{base}}$  are the same parameters of the baseplate.

$$\beta = k \left( \frac{H_H}{\rho_{\text{fb}} V_c^2} \right)^{\frac{1}{2}} \quad (6)$$

$k$  is a constant related to the surface roughness and cleanliness,  $H_H$  is the hardness of the harder material (Pa), and  $\rho_{\text{fb}}$  is the average density of the welded materials ( $\text{kg}\cdot\text{m}^{-3}$ ).

$$V_p = \frac{1}{N} \frac{(T_{\text{Mflyer}} C_{\text{Bflyer}})^{\frac{1}{2}} (\lambda_{\text{flyer}} c_{\text{flyer}} C_{\text{Bflyer}})^{\frac{1}{4}}}{V_c (\rho_{\text{flyer}} \delta_{\text{flyer}})^{\frac{1}{4}}} \quad (7)$$

$T_{\text{Mflyer}}$  is the melting temperature ( $^{\circ}\text{C}$ ),  $C_{\text{Bflyer}}$  is the bulk sound speed ( $\text{m}\cdot\text{s}^{-1}$ ),  $\lambda_{\text{flyer}}$  is the thermal conductivity ( $\text{W}\cdot\text{m}^{-1}\cdot\text{K}^{-1}$ ),  $c_{\text{flyer}}$  is the specific heat ( $\text{J}\cdot\text{kg}^{-1}\cdot\text{K}^{-1}$ ),  $\delta_{\text{flyer}}$  is the

thickness (m), and  $N$  is a constant [41]. All these parameters concern the flyer plate.

Figure 5 illustrates the weldability windows of Al/Cu (grey area) and Cu/Al (green area) configurations. The windows concern dissimilar welds in the same alloys, with the same thickness. From the figure, it can be observed that the theoretical weldable area obtained for Al/Cu joining is larger than that obtained for Cu/Al joining. The difference between both windows results from differences in *Wittman's* and *Walsh's* limits. The wider *Wittman's* limit in Al/Cu welding indicates that this configuration presents a lower susceptibility to excessive interfacial melting. Regarding *Walsh's* limit, it is also wider in the Al/Cu configuration. However, it has no practical effect, as it corresponds to much higher velocities than those obtained with the most common explosive mixtures. Even though these theoretical results indicate a higher weldability when the Al alloy is positioned as the flyer plate, the experimental results showed the opposite (Figs. 1 and 2). However, it should be stressed that the thickness of the baseplate is not considered in any of the weldability equations (Eqs. 5 to 7), which is an important limitation of this analytical tool. This is particularly relevant for welding scenarios in which the thickness of the baseplate is a variable, as in the present research.

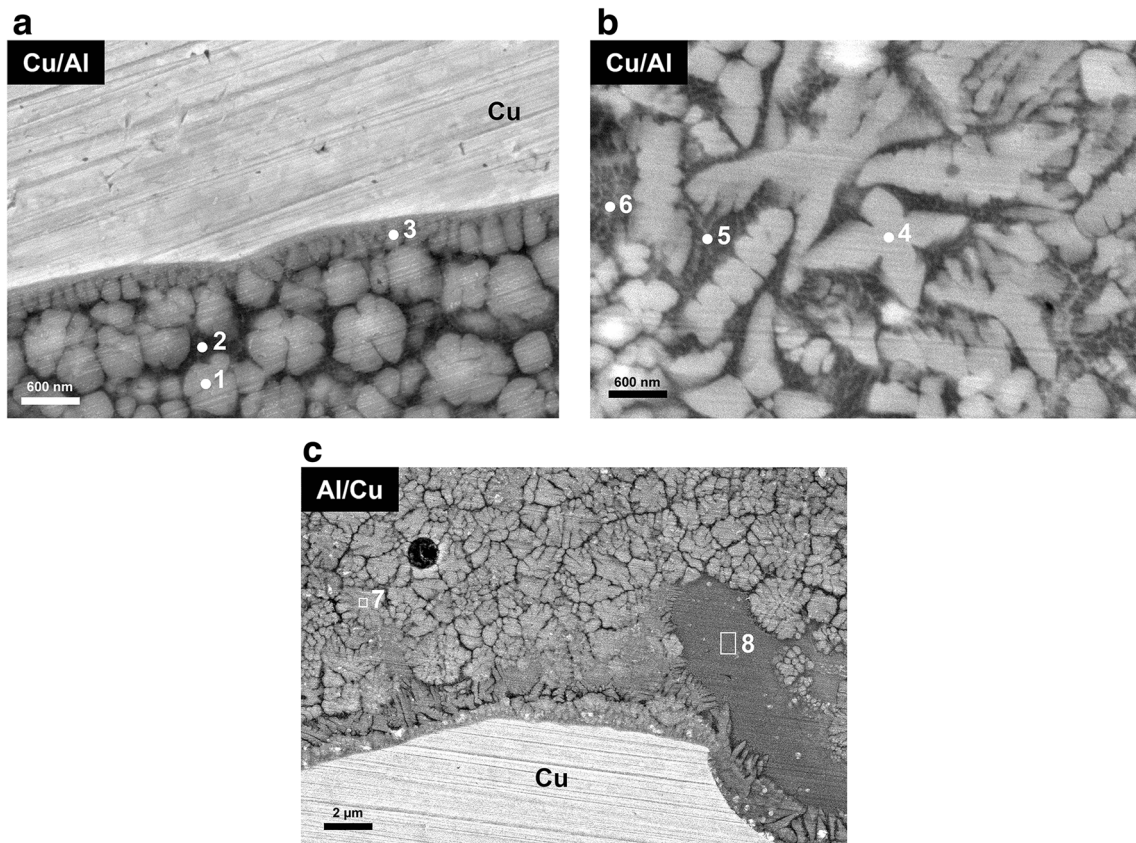


Fig. 4 Microstructural details of the weld interface. a, b Cu/Al weld. c Consistent Al/Cu weld

As reported above, the after-impact failure in Al/Cu welding resulted from two factors: high collision point velocity and high interfacial energy. Both factors favoured continuous interfacial melting, which is related to the upper limit of the weldability window. As an alternative to Wittman’s condition, another theory was developed by Zakharenko [42] and Efremov and Zakharenko [43]. These authors stated that successful interfacial bonding is achieved when the time-relation condition presented in Eq. 8 is respected. According to them, the appearance of positive pressures at the weld interface before the full solidification of the molten material prevents the bonding of the adjoining surfaces of the flyer and the baseplate.

$$t_p \geq t_s \tag{8}$$

$t_p$  is the time required for the appearance of tensile stresses (positive pressures) at the weld interface and  $t_s$  is the time for the solidification of the interfacial molten material. The  $t_p$  and  $t_s$  parameters are calculated using Eqs. 9 to 11.

**Table 5** EDS-based chemical composition (at.%) of the interface of the Cu/Al and Al/Cu welds

Weld	Analysis zones	Al	Cu
Cu/Al	1	65.8	28.2
	2	55.5	42.3
	3	38.9	59.6
	4	64.8	33.0
	5	73.4	20.5
	6	77.0	17.2
Al/Cu	7	62.5	36.1
	8	75.8	22.9

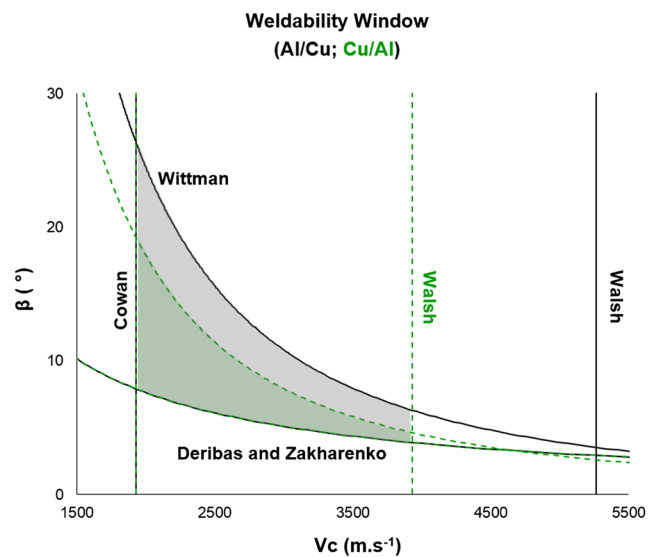
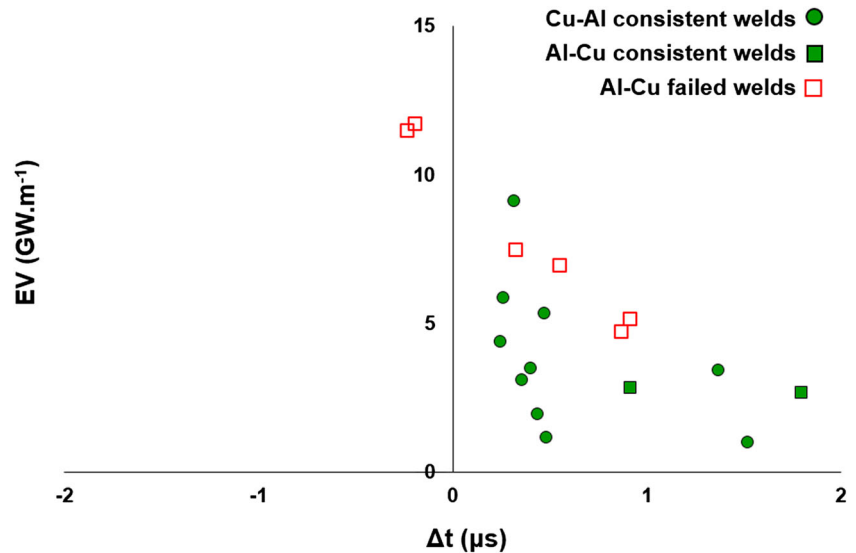


Fig. 5 Weldability windows of Al/Cu (grey) and Cu/Al (green) welding

**Fig. 6** EV vs  $\Delta t$  evolution for the Al/Cu and Cu/Al welds



$$t_p = \left[ 0.5 + 0.66 \left( \frac{\rho_{\text{flyer}} V_c^2}{G_{\text{flyer}}} \right) \right] \frac{\delta_{\text{flyer}}}{V_c} \tag{9}$$

$G_{\text{flyer}}$  is the shear modulus (Pa) of the flyer plate.

$$t_s = \frac{Q^2}{4\pi C_{\text{flyer}} \rho_{\text{flyer}} \lambda_{\text{flyer}} T_{\text{Mflyer}}^2} \tag{10}$$

$$Q = 6.8 \times 10^{-2} V_c^2 \rho_{\text{flyer}} \delta_{\text{flyer}} \frac{\delta_{\text{base}}}{\delta_{\text{flyer}} + \delta_{\text{base}}} \text{sen}^2 \left( \frac{\beta}{2} \right) \tag{11}$$

$Q$  is the heat released at the weld interface (J·m<sup>-2</sup>).  $\delta_{\text{base}}$  is the thickness of the baseplate (m).

Unlike *Wittman's* condition, this theory has the advantage of considering the influence of both the flyer and the baseplate thicknesses on the welding conditions. As shown in Fig. 6, the EV values of the welds were plotted against the difference between the  $t_p$  and  $t_s$  values ( $\Delta t = t_p - t_s$ ). A positive value of  $\Delta t$  indicates that consistent joining is expected, while a negative value means the reverse. From the figure, it can be observed that, although six Al/Cu welds failed (red squares), only two of these welds were expected to fail. On the other hand, none of the Cu/Al welds were expected to fail (green circles), which matches well the welding results. In good agreement with that observed using *Wittman's* condition, the weldability of the Al/Cu configuration is lower than the theoretical weldability obtained by Eqs. 9 to 11.

### 3.4 Limitations of the weldability theories

The main result of the present research regards the mismatch observed between the theoretical weldability of the welded combination and the experimental results. Unlike what was expected based on the theoretical approaches, only the Cu/

Al configuration allowed the production of consistent joints using either low or high EV values. In good agreement with these results, Amani and Soltanieh [44] and Carvalho et al. [4] reported the production of consistent Cu/Al welds using high collision point velocities (3500–4500 m·s<sup>-1</sup>). Table 6 shows the comparison between the Efremov and Zakharenko's theory illustrated in Fig. 6 and experimental results for the aluminium-flyer welds. The theory fails to address the failure of some experiments with high collision point velocities.

Table 7 summarises the experimental results found in the literature concerning similar and dissimilar welding of Al flyer plates. The relative physical properties of the combinations, which are the ratios between the physical properties of each material, are displayed in the table. The ratios were obtained through the division of the higher by the lower value of each property, regardless of whether they correspond to the flyer or the baseplate. The properties addressed in the table are those most affecting the weldability. From the table, it can be observed that when an Al flyer is welded to a baseplate with similar properties (Al and Mg), consistent joints can be achieved using both low and high collision point velocities.

**Table 6** Comparison of Efremov and Zakharenko's theory and experimental results

Al-Cu Welds	Efremov and Zakharenko's theory	Experimental
3Al/3Cu-1	Consistent	Consistent
3Al/3Cu-2	Consistent	Failed
3Al/3Cu-3	Consistent	Failed
3Al/3Cu-4	Consistent	Failed
3Al/3Cu-5	Failed	Failed
3Al/3Cu-6	Failed	Failed
3Al/3Cu-7	Consistent	Failed
5Al/3Cu-1	Consistent	Consistent



**Table 7** Results of explosive welding between Al flyers and different baseplates

Combin.	$V_c$ (m·s <sup>-1</sup> )	Density ratio	Melting temp. ratio	Thermal cond. ratio	Welds	Works
Al/Al*	3523	1.0	1.0	1.0	Consist.	Carvalho et al. [4]
	3477				Consist.	Carvalho et al. [4]
Al/Mg*	3200	1.6	1.0	1.5	Consist.	Chen et al. [45]
	2500				Consist.	Zhang et al. [11]
	2300–2800				Consist.	Zhang et al. [8]
Al/Cu	3589	3.3	1.6	1.7	Failed	Carvalho et al. [3]
	2077				Consist.	Carvalho et al. [3]
	2500–2700				Consist.	Ashani and Bagheri [46]
Al/Fe	2300	2.9	2.3	3.0	Consist.	Li et al. [22]
Al/SS	2300	3.0	2.1	14.6	Consist.	Carvalho et al. [23]
	2077				Consist.	Carvalho et al. [23]
	2600				Consist.	Guo et al. [25]
Al/Ti	1900–1950	1.7	2.5	10.8	Consist.	Fronczek et al. [17]
Al/Ta	2000	6.1	4.5	4.1	Consist.	Greenberg et al. [47]

\*Welds of materials with similar characteristics allowed consistent welds with high collision point velocities (approximately > 3000 m·s<sup>-1</sup>)

Otherwise, when significant differences in density and melting temperature exist between the welded alloys (Fe, SS, Cu, Ti, and Ta), only the tests using low collision point velocities (lower than 3000 m·s<sup>-1</sup>) resulted in consistent welds.

The analysis of the table shows that the reduced weldability of the Al/Cu configuration is not only related to the flyer, but to the combined properties of both welded metals. However, the existing theories for the upper limit of the weldability window [40, 42, 43], which are largely used in dissimilar welding literature, only consider the physical properties of the flyer plate. The properties of both welded metals, or even the difference in these properties, should be considered in these equations. Moreover, *Wittman's* limit also neglects the influence of the baseplate's thickness on the welding conditions, which may influence the results predicted.

A more restrictive limit should be developed to match the welding requirements in Al/Cu welding. In good agreement with this, Carvalho et al. [4] showed that *Cowan's* limit (left limit of the weldability window) in dissimilar welding should be complemented with an analysis of the wave interface factor (WIF). In addition to the difference in the physical properties of the welded materials, the formation of intermetallic regions at the weld interface should also be considered in dissimilar combinations that form intermetallic phases easily. In agreement with Carvalho et al. [19], as the properties of these phases differ from those of the welded metals, the required rearrangement of the existing equations should also include the properties of these phases. This requires a strong characterisation of the intermetallic phases formed in Al/Cu and Cu/

Al welding, specifically, concerning the volume, distribution, and the type of the phases formed in each configuration.

## 4 Conclusions

The aim of the present research was to conduct a broad analysis of the weldability of the aluminium-copper combination by EXW. A large number of welds produced under different welding conditions were analysed. The following conclusions were reached:

- The weldability of the aluminium-copper combination is increased by positioning the copper as the flyer plate and the aluminium alloy as the baseplate;
- When the aluminium alloy is welded as the flyer plate, continuous interfacial melting occurs more easily, i.e. under lower values of energy lost by the collision and collision point velocities;
- The existing theories and equations defining the process requirements for achieving consistent welds, despite being widely used in the dissimilar welding literature, present several limitations concerning aluminium-copper welding;
- Considering the mismatch between experimental and theoretical results, for aluminium-copper welding, new approaches considering the properties of both welded metals, and/or their differences, and the formation of intermetallic phases at the weld interface should be developed.

**Funding information** This research is sponsored by FEDER funds through the programme COMPETE - *Programa Operacional Factores de Competitividade* - and by national funds through FCT - *Fundação Portuguesa para a Ciência e a Tecnologia*, under the project UID/EMS/00285/2013. The authors also acknowledge the financial support of the IPL - *Instituto Politécnico de Lisboa*, under the project IPL/2017/EWDMat/ISEL. The first author, G.H.S.F.L. Carvalho, is supported by CNPq - *Conselho Nacional de Desenvolvimento Científico e Tecnológico (Brazil)*.

## References

- El-Sobky H (1983) Mechanics of explosive welding. In: Blazynski TZ (ed) *Explosive Welding, Forming and Compaction*. Applied Science Publishers, Essex, pp 189–217
- Mousavi AAA, Al-Hassani STS (2005) Numerical and experimental studies of the mechanism of the wavy interface formations in explosive/impact welding. *J Mech Phys Solids* 53:2501–2528
- Carvalho GHSFL, Galvão I, Mendes R, Leal RM, Loureiro A (2018) Influence of base material properties on copper and aluminium-copper explosive welds. *Sci Technol Weld Join* 23(6): 501–507
- Carvalho GHSFL, Mendes R, Leal RM, Galvão I, Loureiro A (2017) Effect of the flyer material on the interface phenomena in aluminium and copper explosive welds. *Mater Des* 122:172–183
- Loureiro A, Mendes R, Ribeiro JB, Leal RM, Galvão I (2016) Effect of explosive mixture on quality of explosive welds of copper to aluminium. *Mater Des* 95:256–267
- Athar MMH, Tolaminejad B (2015) Weldability window and the effect of interface morphology on the properties of Al/Cu/Al laminated composites fabricated by explosive welding. *Mater Des* 86: 516–525
- Paul H, Litynska-Dobrzynska L, Prazmowski M (2013) Microstructure and phase constitution near the interface of explosively welded aluminum/copper plates. *Metall Mater Trans A* 44(8):3836–3851
- Zhang T, Wang W, Zhang W, Wei Y, Cao X, Yan Z, Zhou J (2018) Microstructure evolution and mechanical properties of an AA6061/AZ31B alloy plate fabricated by explosive welding. *J Alloys Compd* 735:1759–1768
- Fronczek DM, Chulist R, Litynska-Dobrzynska L, Kac S, Schell N, Kania Z, Szulc Z, Wojewoda-Budka J (2017) Microstructure and kinetics of intermetallic phase growth of three-layered A1050/AZ31/A1050 clads prepared by explosive welding combined with subsequent annealing. *Mater Des* 130:120–130
- Arisova VN, Trykov YP, Slautin OV, Ponomareva IA, Kondakov AE (2015) Effect of heat treatment on mechanical properties and phase composition of magnesium-aluminum composite prepared by explosive welding. *Met Sci Heat Treat* 57(5–6):291–294
- Zhang N, Wang W, Cao X, Wu J (2015) The effect of annealing on the interface microstructure and mechanical characteristics of AZ31B/AA6061 composite plates fabricated by explosive welding. *Mater Des* 65:1100–1109
- Guo X, Ma Y, Jin K, Wang H, Tao J, Fan M (2017) Effect of stand-off distance on the microstructure and mechanical properties of Ni/Al/Ni laminates prepared by explosive bonding. *J Mater Eng Perform* 26(9):4235–4244
- Bataev IA, Ogneva TS, Bataev AA, Mali VI, Esikov MA, Lazurenko DV, Guo Y, Junior AMJ (2015) Explosively welded multilayer Ni-Al composites. *Mater Des* 88:1082–1087
- Chulist R, Fronczek DM, Szulc Z, Wojewoda-Budka J (2017) Texture transformations near the bonding zones of the three-layer Al/Ti/Al explosively welded clads. *Mater Charact* 129:242–246
- Fan M, Yu W, Wang W, Guo X, Jin K, Miao R, Hou W, Kim N, Tao J (2017) Microstructure and mechanical properties of thin-multilayer Ti/Al laminates prepared by one-step explosive bonding. *J Mater Eng Perform* 26(1):277–284
- Bazamik P, Adamczyk-Cieślak B, Gałka A, Płonka B, Snieżek L, Cantoni M, Lewandowska M (2016) Mechanical and microstructural characteristics of Ti6Al4V/AA2519 and Ti6Al4V/AA1050/AA2519 laminates manufactured by explosive welding. *Mater Des* 111:146–157
- Fronczek DM, Wojewoda-Budka J, Chulist R, Sypien A, Korneva A, Szulc Z, Schell N, Zieba P (2016) Structural properties of Ti/Al clads manufactured by explosive welding and annealing. *Mater Des* 91:80–89
- Lazurenko DV, Bataev IA, Mali VI, Bataev AA, Maliutina IN, Lozhkin VS, Esikov MA, Jorge AMJ (2016) Explosively welded multilayer Ti-Al composites: structure and transformation during heat treatment. *Mater Des* 102:122–130
- Carvalho GHSFL, Galvão I, Mendes R, Leal RM, Loureiro A (2018) Formation of intermetallic structures at the interface of steel-to-aluminium explosive welds. *Mater Charact* 142:432–442
- Guo X, Wang H, Liu Z, Wang L, Ma F, Tao J (2016) Interface and performance of CLAM steel/aluminum clad tube prepared by explosive bonding method. *Int J Adv Manuf Technol* 82:543–548
- Aizawa Y, Nishiwaki J, Harada Y, Muraishi S, Kumai S (2016) Experimental and numerical analysis of the formation behavior of intermediate layers at explosive welded Al/Fe joint interfaces. *J Manuf Process* 24(1):100–106
- Li X, Ma H, Shen Z (2015) Research on explosive welding of aluminum alloy to steel with dovetail grooves. *Mater Des* 87: 815–824
- Carvalho GHSFL, Galvão I, Mendes R, Leal RM, Loureiro A (2018) Explosive welding of aluminium to stainless steel. *J Mater Process Technol* 262:340–349
- Shiran MKG, Khalaj G, Pouraliakbar H, Jandaghi M, Bakhtiari H, Shirazi M (2017) Effects of heat treatment on the intermetallic compounds and mechanical properties of the stainless steel 321-aluminum 1230 explosive-welding interface. *Int J Miner Metall Mater* 24:1267–1277
- Guo X, Fan M, Wang L, Ma F (2016) Bonding interface and bending deformation of Al/316LSS clad metal prepared by explosive welding. *J Mater Eng Perform* 25(6):2157–2163
- Xunzhong G, Jie T, Wentao W, Huaguan L, Chen W (2013) Effects of the inner mould material on the aluminium-316L stainless steel explosive clad pipe. *Mater Des* 49:116–122
- Mendes R, Ribeiro J, Plaksin I, Campos J, Tavares B (2014) Differences between the detonation behavior of emulsion explosives sensitized with glass or with polymeric micro-balloons. *J Phys Conf Ser* 500:1–6
- Mendes R, Ribeiro J, Plaksin I, Campos J (2012) Non ideal detonation of emulsion explosives mixed with metal particles. *AIP Conf Proc* 1426:267–270
- Mendes R, Ribeiro JB, Loureiro A (2013) Effect of explosive characteristics on the explosive welding of stainless steel to carbon steel in cylindrical configuration. *Mater Des* 51:182–192
- Kennedy JE (1970) Gurney energy of explosives: Estimation of the velocity and impulse imparted to driven metal. Sandia National Laboratories, New Mexico
- Cooper PW (1996) *Explosives engineering*. Wiley-VCH, USA
- Hokamoto K, Izuma T, Fujita M (1993) New explosive welding technique to weld aluminum alloy and stainless steel plates using a stainless steel intermediate plate. *Metall Mater Trans A* 24(10): 2289–2297
- Hokamoto K, Chiba A, Nishida M, Fujita M (1995) Experimental conditions for fabrication of multilayered metal base composites by single-shot explosive welding. *Weld Int* 9(2):116–120
- ASM (1992) *Binary phase diagrams*. ASM handbook, vol 3 - Alloy Phase Diagrams. ASM International, Materials Park, Ohio, USA

35. Wulff FW, Breach CD, Stephan D, Saraswati T, Dittmer KJ (2004) Characterisation of intermetallic growth in copper and gold ball bonds on aluminium metallization. Paper presented at the 6th Electronics Packaging Technology Conference (EPTC 2004) (IEEE Cat. No.04EX971), Singapore, 348–353
36. Ribeiro JB, Mendes R, Loureiro A (2014) Review of the weldability window concept and equations for explosive welding. *J Phys Conf Ser* 500:1–6
37. Cowan GR, Bergmann OR, Holtzman AH (1971) Mechanism of bond zone wave formation in explosion-clad metals. *Metall Trans A* 2(11):3145–3155
38. Walsh JM, Shreffler RG, Willig FJ (1953) Limiting conditions for jet formation in high velocity collisions. *J Appl Phys* 24(3):349–359
39. Deribas AA, Zakharenko ID (1974) Surface effects with oblique collisions between metallic plates. *Combust Explos Shock Waves* 10(3):358–367
40. Carpenter SH, Wittman RH (1975) Explosion welding. *Annu Rev Mater Sci* 5:177–199
41. Rosset WSD (2006) Analysis of explosive bonding parameters. *Mater Manuf Process* 21(6):634–638
42. Zakharenko ID (1972) Critical conditions in detonation welding. *Fiz Goreniya Vzryva* 8(3):422–427
43. Efremov VV, Zakharenko ID (1976) Determination of the upper limit to explosive welding. *Fiz Goreniya Vzryva* 12(2):255–260
44. Amani H, Soltanieh M (2016) Intermetallic phase formation in explosively welded Al/cu bimetal. *Metall Mater Trans B Process Metall Mater Process Sci* 47:2524–2534
45. Chen P, Feng J, Zhou Q, An E, Li J, Yuan Y, Ou S (2016) Investigation on the explosive welding of 1100 aluminum alloy and AZ31 magnesium alloy. *J Mater Eng Perform* 25(7):2635–2641
46. Ashani JZ, Bagheri SM (2009) Explosive scarf welding of aluminum to copper plates and their interface properties. *Mat-wiss u Werkstofftech* 40(9):690–698
47. Greenberg BA, Ivanov MA, Rybin VV, Elkina OA, Antonova OV, Patselov AM, Inozemtsev AV, Plotnikov AV, Volkova AY, Besshaposnikov YP (2013) The problem of intermixing of metals possessing no mutual solubility upon explosion welding (Cu-Ta, Fe-Ag, Al-Ta). *Mater Charact* 75:51–62

**Publisher's note** Springer Nature remains neutral with regard to jurisdictional claims in published maps and institutional affiliations.